

1           **CRISPR-Powered Portable Electrochemical Sensing System for Mpox Virus**  
2           **Detection in Environmental Samples**

3       Xiaoyun Zhong<sup>1,2#</sup>, Ijaz Gul<sup>2,3,4#,\*</sup>, Xi Yuan<sup>2,3#</sup>, Muhammad Akmal Raheem<sup>2</sup>, Ke Lin<sup>1,2</sup>,  
4       Chenying lv<sup>1</sup>, Junguo Hui<sup>1</sup>, Shuiwei Xia<sup>1</sup>, Minjiang Chen<sup>1</sup>, Min Xu<sup>1</sup>, Lin Shen<sup>1</sup>, Zhenglin  
5       Chen<sup>1</sup>, Chenggang Yan<sup>3,4</sup>, Peiwu Qin<sup>1,2,3,4\*</sup>, Dongmei Yu<sup>1,3,5\*</sup>, Jiansong Ji<sup>1\*</sup>

6       <sup>1</sup> Lishui Central Hospital, Wenzhou Medical University, Lishui, P. R. China

7       <sup>2</sup> Institute of Biopharmaceutical and Health Engineering, Tsinghua Shenzhen International Graduate School,  
8       Tsinghua University, Shenzhen, P. R. China

9       <sup>3</sup> Lishui Research Institute of Hangzhou Dianzi University, Hangzhou Dianzi University, Hangzhou, P. R.  
10      China

11      <sup>4</sup> School of Communication Engineering, Hangzhou Dianzi University, Hangzhou, P. R. China

12      <sup>5</sup> School of Mechanical, Electrical & Information Engineering, Shandong University, Weihai, Shandong,  
13      China

14      \*Correspondence: **Peiwu Qin**, Institute of Biopharmaceutical and Health Engineering, Tsinghua Shenzhen International  
15      Graduate School, Tsinghua University, Shenzhen 518055, PR China.

16      E-mail address: [pwqin@sz.tsinghua.edu.cn](mailto:pwqin@sz.tsinghua.edu.cn); **Ijaz Gul**, Institute of Biopharmaceutical and Health Engineering, Tsinghua  
17      Shenzhen International Graduate School, Tsinghua University, Shenzhen 518055, PR China

18      E-mail address: [gul.ijaz@sz.tsinghua.edu.cn](mailto:gul.ijaz@sz.tsinghua.edu.cn); [ejazgul786@hotmail.com](mailto:ejazgul786@hotmail.com); **Dongmei Yu**: School of Mechanical, Electrical  
19      & Information Engineering, Shandong University, Weihai, Shandong, China. E-mail address: [yudongmei@sdu.edu.cn](mailto:yudongmei@sdu.edu.cn);

20      **Jiansong Ji**: Lishui Central Hospital, Wenzhou Medical University, Lishui, P. R. China. E-mail address:

21      [jjstcty@wmu.edu.cn](mailto:jjstcty@wmu.edu.cn)

22      <sup>#</sup> Co-first authors

23

24 **Abstract**

25 As clinical testing of mpox virus (MPXV) declines, wastewater testing can be a useful  
26 approach to monitor the undetected MPXV transmission at community level. In this study,  
27 we report a prototype biosensing system for wastewater-based surveillance of mpox virus.  
28 We fabricated a DNA-modified electrode and employed CRISPR/Cas12a as a  
29 biocomponent for accurate recognition of viral DNA and subsequent cleavage of the  
30 reporter DNA immobilized on electrode surface to influence signal transduction. The data  
31 is collected through a cloud-supported system on smartphone and can be remotely accessed.  
32 For environmental sample detection, we used mpox pseudovirus to prepare simulated  
33 samples in river and sea waters to demonstrate the practical utility of the proposed system.  
34 The system can detect viral DNA down to pM level without target amplification. The  
35 biosensor demonstrated promising recoveries ranging from 85-103% when challenged  
36 with spiked environmental samples. Our internet of things-supported wastewater  
37 surveillance system takes mpox diagnostic to the next level where a single test could inform  
38 about the disease scale and prevalence at community level earlier than the clinical testing.  
39 Further, the developed approach has a potential application value in scenarios where  
40 disease has a sexual transmission route, and individuals hesitate to participate in clinical  
41 testing due to the fear of stigmatization.

42 **Keywords:** MPXV, Wastewater epidemiology, CRISPR/Cas12a, internet of things,  
43 Environmental biosensing

44

45 **1. Introduction**

46 Mpoxy is a contagious disease caused by mpox virus (MPXV). Since May 2022, large  
47 number of Mpoxy cases have been reported in non-endemic countries which lead to the  
48 declaration of public health emergency of international concern by WHO in July, 2022 [1,2]  
49 and remained in effect until May, 2023 [3,4]; prompting surge in mpox research worldwide.  
50 MPXV harbors double-stranded DNA as a genetic material, and is classified into *Orthopox*  
51 genus and *Poxviridae* family[5,6]. The virus is mainly transmitted by close contact with  
52 infected persons and body fluids; the transmission by aerosols and fomite transmission  
53 have also been anticipated [7]. Although there is a relatively slower increase in mpox cases  
54 worldwide, timely detection of MPXV is crucial to prevent its undetected transmission and  
55 future outbreaks.

56 Mpoxy positive persons shed viral particles or DNA in urine, stool, and skin lesions [8,9];  
57 thus, can release virus into the environmental waters through urinating, defecating,  
58 showering, or releasing seminal fluid into water [10]. Based on this assumption, several  
59 reports claimed the presence of MPXV DNA in environmental water samples [11–16]; [17],  
60 underscoring the importance of wastewater epidemiology. Wastewater surveillance for  
61 MPXV detection can help public health authorities to track virus infections in a particular  
62 population without testing individual cases, where the sewage sample can be collected from  
63 a common wastewater outlet. Several MPXV detection methods have been reported since  
64 May 2022 [18–21]. These detection approaches mainly harness fluorescence and  
65 electrochemical signal transduction modalities. However, electrochemical biosensors are  
66 relatively easy to digitalize, sensitive, integrated, and field deployable [22–24], indicating  
67 their potential for developing novel MPXV diagnostic systems.

68 CRISPR/Cas systems have enticed significant research interest particularly in response to  
69 COVID-19 pandemic [25,26]. Several CRISPR-powered mpox detection systems have  
70 been developed with commendable sensitivities and selectivities [18,21,27–30]. However,  
71 most of these detection methods rely on target pre-amplification which involves complex  
72 machinery, thereby increasing assay cost and time. Amplification-free detection is a  
73 promising alternative. In this regard, several strategies have been explored to develop

amplification-free detection of MPXV, including multiple crRNAs combination [31], aptasensors-based detection [29], electrochemical impedance-based mpox antigen detection [32], graphene quantum rods-based antigen sensing [33], CRISPR/Cas12b-empowered graphene field effect transistor (gFET) for MPXV detection [27], and detection based on nanopore sensing strategy [34], etc. Although promising and sensitive, the methods solely focus on mpox detection in biofluids. Currently, MPXV in wastewater samples is detected by quantitative polymerase chain reaction (qPCR). Although sensitive and universal, the qPCR is expensive, laborious, needs expert technicians, hard to employ in resource-limited settings and lacks field deployability, emphasizing the need for developing a state-of-the-art system for mpox wastewater epidemiology.

Herein, we developed a CRISPR/Cas-powered and IoT-supported system for MPXV detection in wastewaters. We modified screen printed gold electrode with several DNA reporters and harnessed CRISPR/Cas-12a for target recognition and cleavage of the reporter immobilized on electrode surface. The data is collected through a cloud-supported system on smartphone and can be remotely accessed. For environmental sample detection, we used mpox pseudovirus to prepare simulated samples in river and sea waters and demonstrated the practical utility of our system.

## 2. Materials and Methods

### 2.1. Materials and Reagents

Nucleic acid sequences including crRNAs (B7R and F3L), DNA targets, control, DNA reporters, and PCR primers shown in **Table S1** were synthesized by Sangon Biotech Co., Ltd. (Shanghai, China). MPXV F3L gene pseudovirus (**Table S1**) was also procured from Sangon Biotech Co., Ltd. (Shanghai, China). EnGen® Lba (*Lachnospiraceae bacterium*) Cas12a (Cpf1) and 10× NEBuffer 2.1 were purchased from New England Biolabs Inc. (Beijing, China). Other reagents, such as NaCl, K<sub>3</sub>[Fe(CN)<sub>6</sub>], K<sub>4</sub>[Fe(CN)<sub>6</sub>], KCl, Tris-(2-carboxyethyl) phosphine hydrochloride (TCEP), 6-mercaptophexanol (MCH), 10× phosphate-buffered saline (PBS) solution, 10× Tris-borate-EDTA (TBE) solution, SYBR Green II, and 6× DNA loading buffer were supplied by Solarbio Tech. Co., Ltd. (Beijing, China). 20 bp DNA Ladder was sourced from Takara Biomed. Inc. (Beijing, China). The PCR amplification kit, gel extraction kit, and PCR purification kit were provided by

104 Beyotime Co., Ltd. (Shanghai, China). The SPARKeasy viral genomic DNA extraction kit  
105 was obtained from Sparkjade Co., Ltd. (Jinan, China). All reagents were of analytical grade  
106 and used as provided without further purification. DNase/RNase-free purified water was  
107 used in all experiments. Human saliva was collected from a healthy volunteer with  
108 informed consent. The river water was collected from Pearl River, Foshan, China from two  
109 different sites (termed river-1 and river-2), and sea water was collected from South China  
110 Sea. Water samples were filtered by a 0.4 µm membrane and used to prepare mocked  
111 samples.

112 Flame retardant 4 (FR-4) printed circuit board (PCB) screen-printed-electrodes (SPEs)  
113 were procured from Mecart Sensor Tech. Inc. (Guangzhou, China). The SPE is comprised  
114 of three electrodes including, gold as a working electrode (with a working area of 23.75  
115 mm<sup>2</sup>), carbon as a counter electrode, and Ag/AgCl as a reference electrode. All differential  
116 pulse voltammetry (DPV) measurements were conducted using a portable potentiostat  
117 (BIOSYS-RIT-P15-001) obtained from Shenzhen Refresh Biosensing Technology Co.,  
118 Ltd. (Shenzhen, China) along with a cloud-supported system. While electrochemical  
119 impedance spectroscopy (EIS) analysis was carried out with the Ametek EnergyLab XM  
120 Potentiostat Galvanostat (Pennsylvania, USA). A microplate reader (SPARK; TECAN)  
121 was used for fluorescence measurements. The concentration of DNA oligonucleotides was  
122 measured using NanoDrop<sup>TM</sup> 2000 (Massachusetts, USA). Bio-Rad electrophoresis  
123 apparatus was used for gel electrophoresis, and gel was imaged using Bio-Rad  
124 ChemiDoc<sup>TM</sup> MP imaging system (California, USA).

125 All experiments were performed at least in triplicates (technical replicates) unless  
126 otherwise stated and data are presented as the mean ± standard deviation. Data was  
127 analyzed using Microsoft Excel and OriginPro2021.

## 128 **2.2. Fabrication of DNA-modified Electrodes**

129 Three DNA probes with different lengths and structures (one linear and two hairpin) having  
130 thiol group (-SH) at 5' end for Au-S bond and methylene blue (MB) at 3' end serving as a  
131 redox reporter were designed to select the best-performing probe. The screen-printed gold  
132 electrodes were thoroughly washed with ddH<sub>2</sub>O before probe immobilization. The  
133 thiolated MB-DNA probes were reduced (the color transition from blue to colorless) with

134 a freshly prepared TCEP (10 mM). For hairpin DNA (hpDNA) formation, the oligos were  
135 incubated at 65°C for 5 minutes, followed by a gradual decrease in temperature  
136 (1°C/minute) down to 25°C. Subsequently, 45 µL linear or hpDNA probe (1 µM) was then  
137 dropped onto the working electrode and incubated for 12 hours in a humid and dark  
138 environment to form a self-assembled monolayer (SAM) *viz.*, Au-SH-DNA-MB.

139 Following incubation and SAM formation, any excess DNA probes were washed away  
140 with ddH<sub>2</sub>O. The excess water from the electrode was removed by gently wiping it with a  
141 laboratory wipe. After that, 45 µL of fresh 1 mM MCH diluted in 10 mM PBS (pH 7.4)  
142 was added to the working electrode and incubated for 30 minutes to block the unbound  
143 sites on the working electrode to achieve a well-aligned DNA monolayer. Finally, after  
144 thoroughly washing with 10 mM PBS (pH 7.4), the electrodes were stored in dark in air-  
145 free environment created by nitrogen gas.

146 **2.3. CRISPR/Cas12a Assay**

147 The Cas12a-crRNA complex was preassembled by incubating 0.45 µL of 5 µM Cas12a,  
148 0.45 µL of 6.25 µM crRNA, 4.5 µL of 10× NEbuffer, and 24.6 µL of DNase/RNase free  
149 ddH<sub>2</sub>O for 10-15 minutes. The final concentrations of Cas12a and crRNA were maintained  
150 as 50 nM and 62.5 nM, respectively, in a 45 µL reaction system. Subsequently, a 15 µL  
151 DNA target (synthetic DNA or pseudoviral DNA) was added to activate the CRISPR/Cas  
152 complex, followed by an incubation for 15 minutes at 37 °C. The activated complex was  
153 then added dropwise to the working electrode surface and allowed to react for 60-90  
154 minutes at 37 °C. The electrochemical measurements were performed as described below.

155 **2.4. Electrochemical Measurements**

156 After the CRISPR/Cas12a-mediated interfacial cleavage reaction (cleavage of the  
157 immobilized reporter), the electrodes were thoroughly rinsed with ddH<sub>2</sub>O. Then,  
158 differential pulse voltammetry (DPV) was employed using DPV buffer comprising 10 mM  
159 PBS (pH 7.4) and 0.5 M NaCl as the electrolyte. Prior to use, the DPV buffer was purged  
160 with nitrogen gas for 5 minutes to remove oxygen to minimize unwanted redox reactions  
161 possibly caused by oxygen. To assess the cleavage effect of CRISPR/Cas12a system, DPV  
162 measurements were conducted before and after the reaction under following conditions: a  
163 potential ranging from -0.5 to -0.1 V (*vs.* Ag/AgCl), a modulation time of 0.2 s, an interval

164 time of 0.1 s, a step potential of 5 mV, and a modulation amplitude of 50 mV. The  
165 measurements were performed either by covering all three electrodes of SPE with 300  $\mu$ L  
166 of DPV buffer or by immersing the electrode in DPV buffer (no significant difference in  
167 signal occurs provided all three electrodes are completely covered with DPV buffer in both  
168 scenarios). Quantitative analyses were carried out by recording the peak current around -  
169 300 mV as follows:

170 
$$\Delta I (\%) = \frac{(\text{Background Signal} - \text{Target Signal})}{(\text{Background Signal})} \times 100 \%, \quad (1)$$

171 where  $\Delta I (\%)$  is the percent change in current intensity at around -300 mV, background  
172 signal is the DPV signal obtained in the absence of the analyte, while the target signal is  
173 the DPV signal obtained in the presence of the target DNA (synthetic or pseudoviral). Here,  
174 the current signal of both the background and target underwent baseline correction and  
175 peak fitting using Origin2021 software, ensuring accurate analysis and interpretation of the  
176 data.

177 EIS was performed using 5 mM  $[\text{Fe}(\text{CN})_6]^{3-/\text{4}-}$  in 0.1 M KCl solution using a biased  
178 potential of 0.23 V (vs. Ag/AgCl) in the frequency range of 0.01 to  $10^5$  Hz, and a voltage  
179 amplitude of 5 mV. The acquired data are presented in Nyquist plots.

180 **2.5. Nucleic Acid PAGE**

181 The 15% native polyacrylamide gel electrophoresis (PAGE) was employed to assess the  
182 collateral cleavage activity of Cas12a on electrode surface and in the solution system.  
183 Samples for electrophoretic analysis were directly collected from the electrode surface.  
184 Electrophoresis was performed in 1× TBE buffer at 120 V for 60 minutes. Subsequently,  
185 the gel was immersed in a solution containing SYBR Green II and 0.1 M NaCl for 20  
186 minutes to stain nucleic acids. The gel was visualized by Bio-Rad gel documentation  
187 system.

188 **2.6. Evaluation of Practical Utility by Mocked Samples**

189 Monkeypox F3L pseudovirus was introduced into human saliva, tap water (10-fold  
190 dilution), and river water (3-fold dilution). The CRISPR assay was performed as described

191 above for the B7R gene, with crRNA combinations substituted with the optimized F3L-  
192 crRNA-3 and F3L-crRNA-4 (**Table S1**).

193 The viral nucleic acid extraction from simulated samples was performed by adding  
194 pseudovirus to a 3-fold diluted river water to ensure that the viral DNA (if present) from a  
195 real-sample could be extracted. The SPARKeasy Viral Genomic DNA Extraction Kit from  
196 Sparkjade was used to extract DNA according to the manufacturer's protocol. The  
197 extracted product was subsequently PCR-amplified and then diluted into a series of  
198 concentrations to generate a calibration curve. For spike-recovery experiments, the known  
199 concentrations of the amplified pseudovirus DNA were added to other environmental  
200 samples to determine the recovery value using the above calibration curve.

201 **3. Results and Discussion**

202 **3.1. System Setup and Feasibility**

203 As evident by COVID-19 pandemic and recent unprecedented mpox outbreaks, the global  
204 healthcare system needs innovative and smart disease monitoring solutions by integrating  
205 advanced biotechnology, artificial intelligence (AI), and cloud-supported platforms. In this  
206 study, we developed a biosensor that relies on the target-induced *trans*-cleavage activity of  
207 CRISPR/Cas12a to influence the redox reaction on DNA-functionalized gold electrode  
208 surface. The schematic of the workflow of the system is shown in **Fig. 1A**. In the presence  
209 of target DNA, the Cas12a-crRNA-target DNA triplex is formed, triggering both *cis*- and  
210 *trans*-cleavage activities. The activated Cas12a effectively cleaves DNA probes  
211 immobilized on electrode surface, releasing MB from the electrode surface, thereby  
212 reducing the peak current. Without target DNA, the Cas12a remains inactive, maintaining  
213 MB proximity to the electrode surface and generating a substantial redox signal. The  
214 electrode is connected to a portable potentiostat wirelessly connected to a smartphone. The  
215 data is obtained on a smartphone in real-time and stored in a cloud that is remotely  
216 accessible using login details.

217 For feasibility tests, we initially used a linear reporter named single-stranded DNA  
218 (ssDNA). The schematic illustration of the electrode fabrication process is shown in **Fig.**  
219 **1B**. Reporter immobilization and interfacial *trans*-cleavage activity of Cas12a were  
220 evaluated by employing EIS and native PAGE. EIS was performed using 5 mM

[Fe(CN)<sub>6</sub>]<sup>3-/4-</sup> in 0.1 M KCl solution to confirm successful electrode fabrication and CRISPR/Cas12a system cleavage (**Fig. 1 C,D**). The semicircle Nyquist curve represented the charge transfer resistance ( $R_{CT}$ ) on electrode surface[35];[36]. Initially, the bare electrode displayed nearly a straight line (curve a), indicating a fast electron transfer between [Fe(CN)<sub>6</sub>]<sup>3-/4-</sup> and electrode surface. Subsequent immobilization of MB-ssDNA reporter on electrode led to a semicircle curve with a significant increase in  $R_{CT}$  to 5,139  $\Omega$  (curve b) as expected. This increase can be attributed to the hinderance in electron-transfer kinetics caused by immobilized DNA probe, resulting in higher surface impedance. To test the CRISPR-mediated reporter cleavage on electrode surface, we challenged our sensor with activated CRISPR/Cas complex. The cleavage of ssDNA reporter on electrode surface led to a notable decrease in  $R_{CT}$  (decrease in diameter of semicircle cure; curve c). These results indicate the successful reporter immobilization and subsequent cleavage by CRISPR/Cas system. Our EIS results are in line with a previous report where nucleic acid-conjugated redox probe was immobilized on electrode surface [37].

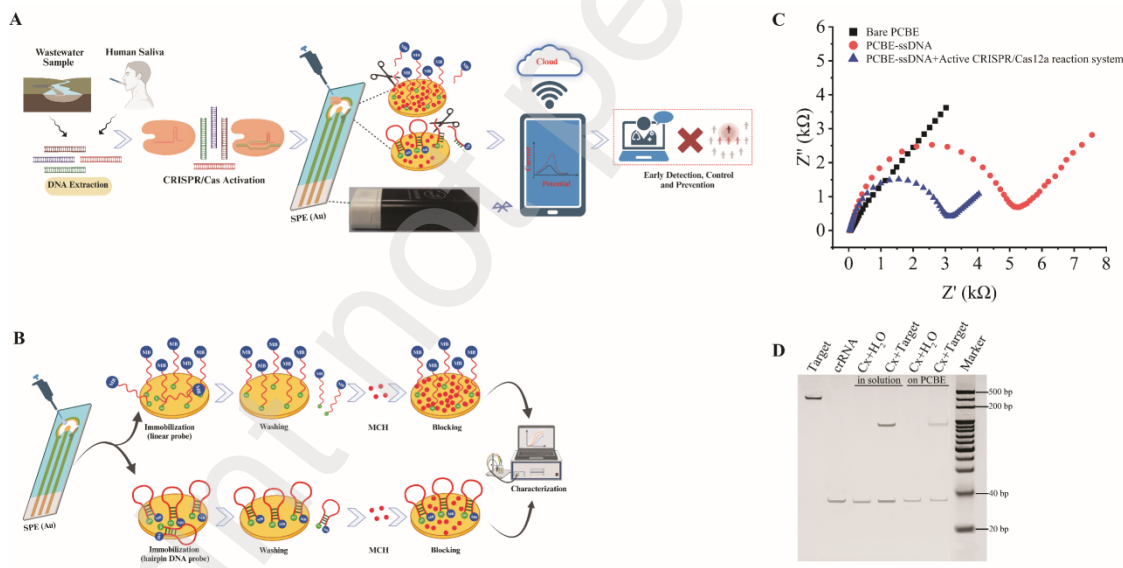


**Fig. 1. System set up and feasibility analysis. (A)** Workflow of the developed Mpoxy virus detection system. “Created with biorender.com”; **(B)** Schematic illustration of the electrode fabrication process. “Created with biorender.com”; **(C)** ssDNA reporter immobilization and CRISPR/Cas-mediated cleavage. EIS of (a) bare PCBE, (b) ssDNA modified PCBE, (c) ssDNA modified PCBE after CRISPR-Cas12a cleavage; **(D)** Image of the Native PAGE. Cx: Cas12a-crRNA.

Native PAGE was employed to visualize the cleavage phenomenon on the electrode surface. Reaction products were collected from different reaction conditions and assessed by PAGE. Although the smaller size and lower concentration of 20 nt ssDNA reporter

made it challenging to visualize on PAGE, the CRISPR-based cleavage of the target DNA could be clearly seen in gel images (**Fig. 1D**, lane 4 and lane 6), both in solution and on the electrode surface, indicating a successful ssDNase activity of Cas12a on electrode surface. The reaction occurring on the electrode surface was first performed on the electrode as described above and then reaction mixture was recollected into the eppendorf tube. As a result, there is a slightly lower concentration of the Cas12a cleavage product displayed on native PAGE compared to the one when the reaction is performed in solution. However, our data reasonably indicate a successful solid-phase activity of CRISPR/Cas12a for biosensor development.

### 3.2. Biosensor Parameter Optimization

The structure of DNA probes immobilized on the electrode surface significantly influences the electrochemical signal, thereby affecting the sensitivity of the biosensor [38,39]. We compared three different probes with different lengths and structures to select the best probe for biosensor development (**Table S1**). As can be seen in **Fig. 2A**, the ssDNA probe yields higher and more stable electrochemical signals compared to hpDNA probes. The hairpin structure is assumed to reduce the distance between the redox probe (MB in our case) and electrode surface, thereby increasing electron transfer rate, and eventually an enhanced sensitivity. However, ssDNA probe outperformed compared to hpDNA probes. DNA structural heterogeneity on electrode surface governs the overall electron transfer between redox probe and electrode [40,41]. The difference in electron-transfer behavior of ssDNA and hpDNA probes might be due to an unequal number of probe molecules immobilized on the electrode surface and steric hinderance caused by hairpin structure due to molecular crowding [41,42]. Further, the ssDNA-based electrode fabrication was highly reproducible (RSD ~ 4.6%, n=10) compared to hpDNA (hpDNA-1) probe (RSD ~ 26.6%, n=10), hence used for biosensor development.

In CRISPR-mediated electrochemical biosensor, the *trans*-cleavage activity of Cas12a serves as a critical component in signal transduction, exerting a profound influence on sensor performance. To optimize *trans*-cleavage activity, the concentration of Cas12a-crRNA complex in a 45 µL reaction system was carefully evaluated. A Cas12a-cRNA molar ratio of 1:1.25 was maintained throughout the experiments while changing the total

concentration of the complex. The concentration of the target (B7R gene) was maintained at 50 nM, and reaction was performed at 37 °C for 1h.  $\Delta I$  (%) changes were compared using different concentrations of Cas12a-crRNA duplexes (Fig. 2B). The Cas12a effector concentration of 50 nM was found to be optimal. Higher concentrations (>50 nM) of Cas12a-crRNA may impede the diffusion and capture of the target, thereby reducing the accessibility of ssDNA reporters to Cas12a endonuclease. Conversely, lower concentrations (<50 nM) might have led to a decreased availability of nucleases for trans-cleavage activity, consequently leading to a decreased signal change. Thus, the optimal concentration of 50 nM is a balance between these factors, ensuring optimal performance of the electrochemical biosensor, and was thus selected as the optimum concentration.

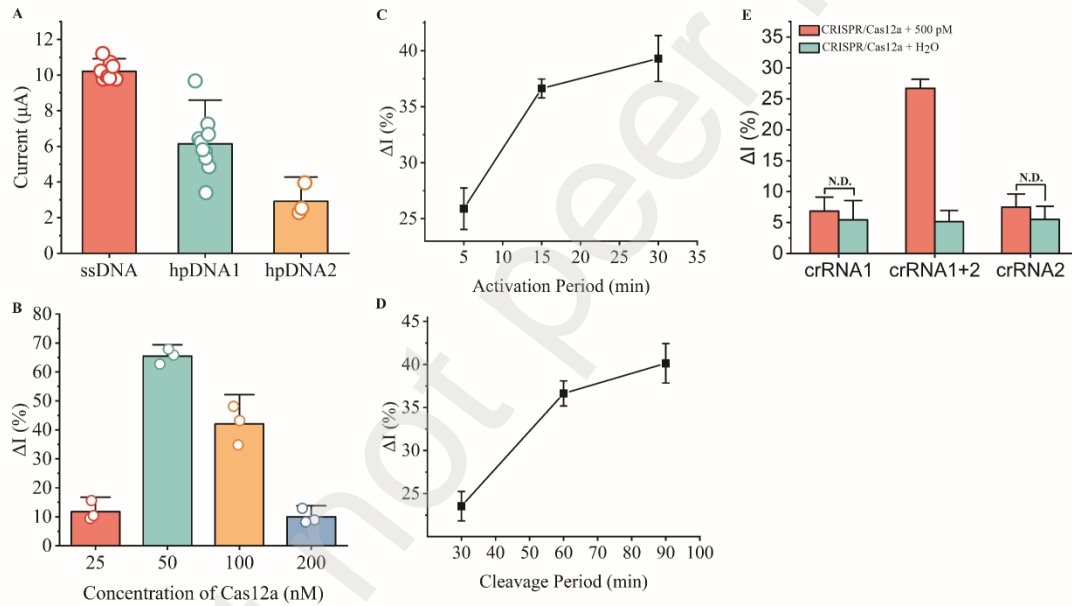


*Fig. 2. Parameter optimization of the proposed system. (A) Effect of probe structural heterogeneity on signal transduction. Standard deviation for ssDNA and hpDNA-1 was calculated from 10 independent repeats, whereas 3 repetitions were performed for hpDNA-2; (B) Optimization of CRISPR/Cas complex concentration. The standard deviation was calculated from three independent replicates ( $n=3$ ); (C) Activation time of Cas12a-crRNA-target complex; (D) Interfacial cleavage time; (E) Evaluation of crRNA combinations for biosensor sensitivity enhancement. The standard deviation was calculated from three independent replicates (C-E).*

Upon crRNA-target DNA hybridization, *cis*- and *trans*-cleavage modes of Cas12a are activated [43]. This process involves early assembly of the Cas12a-crRNA-target triplex and subsequent cleavage. The impact of the triplex incubation time and cleavage time on biosensor performance were investigated separately. Cas12a, crRNA, and 10 nM B7R target gene were assembled in optimized proportions and incubated at 37°C for varying time. The assay mix (containing either active or inactive CRISPR/Cas system) was then

dropped onto the electrode surface (for 1h) for interfacial cleavage (**Fig. 2C**). The maximum *trans*-cleavage activity was found for 15-minute incubation. While above 15 minutes, no significant increase in *trans*-cleavage was observed, suggesting 15 minutes an optimal time for target-induced *trans*-cleavage of the immobilized reporter. We next sought to determine the optimum reporter cleavage time by keeping the activation time constant (15 minutes). The results showed a 60-minutes cleavage time is deemed sufficient for maximal reporter cleavage (**Fig. 2D**).

To further improve the sensitivity of the system, the crRNA combination approach was evaluated, which has been previously demonstrated to significantly enhance the detection sensitivity of the CRISPR/Cas12a reaction in liquid-phase assays [31,44]. This approach involves combining multiple crRNAs into a single group applied for the CRISPR-Cas12a reaction to amplify the signal intensity generated by individual crRNAs. As presented in **Fig. 2E**, the combination of crRNA-1 and crRNA-2 (B7R gene) yields superior cleavage effects on the electrode surface compared to using only one type of crRNA. This enhancement effectively boosts detection sensitivity. To maintain the optimal ratio of Cas12a to crRNA (1:1.25), the total concentration of crRNAs (equimolar) was maintained at 62.5 nM. Since we used B7R and F3L genes in our study. We tested crRNA combinations for F3L gene as well. We designed four crRNAs for F3L gene and screened for the best crRNAs for combination test. As shown in **Fig. S1**, the F3L\_crRNA-3 and F3L\_crRNA-4 outperformed among all tested F3L-crRNAs. Next, we combined F3L\_crRNA-3 and F3L-crRNA-4 to improve signal intensity. The combination of crRNAs increased the signal intensity of the CRISPR/Cas system (**Fig. S2**).

### 3.3. Analytical Performance of the Biosensor

After optimizing the reaction conditions, the analytical performance of the developed CRISPR-powered electrochemical biosensor was assessed. The synthetic B7R gene was diluted in ddH<sub>2</sub>O to prepare a series of dilutions. As shown in **Fig. 3A**, the DPV signal of the MB redox peak gradually weakened within the target concentration range of 50 pM to 50 nM. Further, a concentration dependent linearity was observed between ΔI (%) and logarithm of the target DNA concentration (**Fig. 3B**). The regression equation was derived as  $\Delta I (\%) = 23.57 \lg C + 36.37$ , with a correlation coefficient ( $R^2$ ) value of 0.9972. Due to

314 the logarithmic relationship between the target concentration and the current signal, the  
315 LoD was calculated using four-parameter logistic (4PL) method as follows [32,45]:**Error!**  
316

### Reference source not found.

317  $L_B = \mu_{blank} + t_{(95\%, n-1)} \cdot \sigma_{blank}$  (2)

318  $L_B$  denoting the limit of the blank, holds substantial significance as a critical parameter in  
319 analytical methodology, with a 5% probability for false-positive results. It is determined  
320 through meticulous considerations:  $\mu_{blank}$  represents the mean of signal intensities obtained  
321 from  $n$  replicates (Here,  $n = 10$ ), while  $\sigma_{blank}$  characterizes the standard deviation  
322 associated with the analytical blank. The  $t_{(95\%, n-1)}$  stands for the t-student value  
323 corresponding to  $n - 1$  degrees of freedom, ensuring a 95% confidence level in the  
324 statistical analysis.

325  $LOD = L_B + t_{(95\%, m(n-1))} \cdot \sigma_{test}$  (3)  $\sigma_{test} = \sqrt{\frac{\sum_{i=1}^m \sigma_i^2}{m}}$  (4)  $\sigma_{test}$  is depicted in equation (4):  
326 the pooled standard deviation of  $\Delta I$  values for  $n = 3$  replicates for each point of  
327 concentrations of the curve. Moreover,  $t_{(95\%, m(n-1))}$  represents the t-student value for  
328  $m(n - 1)$  degrees of freedom with a 95% confidence level. These parameters collectively  
329 facilitate precise and reliable determination of  $LoD$  and  $L_B$  values, essential for accurate  
330 analytical assessments.

331 The limit of the blank was calculated from  $n = 10$  replicates, yielding  $\mu_{blank}$  as 2.51% and  
332  $\sigma_{blank}$  as 1.59%. Employing the t-student value  $t_{(95\%, n-1)}$  under a 5% probability for false-  
333 positive results,  $YL_B$  is equal to 6.09%. For the  $YLoD$  is calculated with the pooled standard  
334 deviation of  $\Delta I$  (%) for  $n = 3$  replicates for each point of  $m = 7$  concentrations of the curve.  
335  $t_{(95\%, m(n-1))}$  is reported for the t-student value for  $m(n-1)$  degrees of freedom with 95%  
336 confidence. The calculated  $YLoD$  was found to be 11.24%. Therefore, the LoD was  
337 calculated as 85.88 pM. Notably, this figure of merit aligns with the sensitivity  
338 demonstrated by laboratory-grade optical detection equipment, emphasizing the potential  
339 of our electrochemical biosensor for application in decentralized settings.

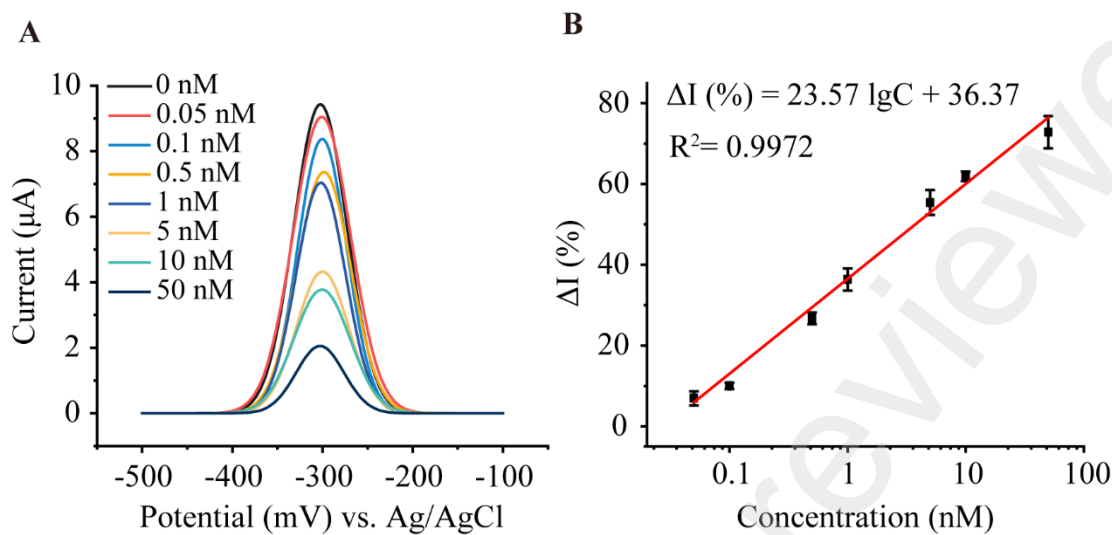


*Fig. 3. Analytical sensitivity of the developed electrochemical biosensor. (A) Representative DPV curves in response to 0, 0.05, 0.1, 0.5, 1, 5, 10, and 50 nM MPXV B7R target. (B) The calibration curve for  $\Delta I$  versus the logarithm of the target DNA concentration. IgC represents the logarithm of the target DNA concentration. Error bars indicate the standard deviation calculated from three independent measurements.*

### 341 3.4. Detection of Simulated Samples Using Developed Biosensor

342 To comprehensively assess the practical utility of our biosensor for virus detection in wastewaters,  
 343 biosensor was challenged with simulated environmental samples. MPXV pseudovirus harboring  
 344 MPXV F3L gene was spiked into various environmental samples, including river water, sea water  
 345 and tap water, mimicking scenarios relevant to wastewater-based epidemiological testing. Since  
 346 the pseudovirus titer was lower than the detection limit of the biosensor, the viral DNA was  
 347 extracted from the spiked sample and used for spike recovery experiments.

348 For a precise quantitative detection, a calibration curve was initially established. The MPXV  
 349 pseudovirus was spiked into river water samples in a 1:3 ratio, and viral DNA was extracted using  
 350 a rapid viral nucleic acid extraction kit. Following extraction, the target DNA was PCR-amplified  
 351 and purified using gel extraction kit (Figure S3). The extracted DNA was diluted to prepare a series  
 352 of concentrations, including 50 nM, 10 nM, 5 nM, 1 nM, 500 pM, 100 pM, and 50 pM. These  
 353 diluted samples were then used to obtain a calibration curve. The regression equation  $\Delta I (\%) =$   
 354  $20.45 \lg C + 30.70$  was obtained, with a  $R^2$  value of 0.9968, and used to quantify the spiked DNA  
 355 in environmental samples (Fig. S4).

356 Initially we spiked a known concentration of DNA into the 50-fold diluted tap water and human  
 357 saliva (to mimic clinical samples). No significant interference was observed compared to the same  
 358 amount of DNA dissolved in NEbuffer (Fig. S5), indicating a potential resistance to the diluted  
 359 real-sample matrices. Since the amount of viral DNA in environmental samples remains lower[10],

360 we used a 1:3 dilution ratio to minimize the real-sample dilution. Subsequently, varying  
361 concentrations of mpox pseudovirus DNA were introduced into diluent environmental samples,  
362 simulating real-world conditions. The recoveries were determined using the developed calibration  
363 curve. Despite a 3-fold sample dilution, excellent recoveries were observed, ranging from 84.99%  
364 to 103.37%, with an RSD ranging from 5.6% to  $\leq$  16%. The biosensor demonstrated reliable  
365 mocked samples results, highlighting its suitability for wastewater-based community level disease  
366 diagnosis and surveillance.

367 Our quantitative mpox virus detection method has the potential to predict the viral load of  
368 a clinical or environmental sample. Previous studies have shown a correlation between  
369 MPXV DNA concentration and viral titers [46–48], potentiating our approach for possible  
370 viral load measurement. Currently, MPXV detection in wastewater is done by PCR-based  
371 amplification methods [12–14]. Although sensitive and versatile, the approach is expensive,  
372 not suitable for resource-limited settings, and lacks portability. Our biosensor is field-  
373 deployable, user-friendly, and integrates IoT for rapid and real-time data access at remote  
374 sites for timely execution of infectious disease prevention and control measures. Several  
375 MPXV detection methods have been recently developed based on electrochemical signal  
376 transduction modality with commendable sensitivities ranging from nM-aM level (Cai et  
377 al., 2023; Can et al., ; Chandran et al., 2024; de Lima et al., 2023; Wang et al., 2023). The  
378 sensitivity of our biosensor is comparable to several previous reports. We developed a  
379 CRISPR/Cas-based molecular detection method while most of the reported MPXV  
380 electrochemical methods target MPXV A29 protein (antigen tests), making them error  
381 prone. However, it is worth mentioning that the approach developed herein needs to be  
382 tested in real-world scenarios before further extending for wastewater epidemiology. The  
383 detection limit of the system can be further improved by harnessing protein engineering  
384 techniques (Gul et al., 2020; Saha et al., 2024; Tong et al., 2024), leveraging the sensing  
385 potential of materials [54](Fan et al., 2022), cascade signal amplification [58], and  
386 harnessing deep learning methods [59,60].

387 **Table 1 Recovery analysis for the simulated samples**

Sample	Concentration of MPXV spiked (nM)	Concentration of MPXV detected (nM)	Recovery (%)	RSD (%)
River-1 (pH=7.8)	5 0.5	5.17 0.48	103.37 95.04	5.95 14.54
River-2	5	4.85	96.95	13.65

(pH=7.9)	0.5	0.44	87.19	13.87
Sea	5	4.58	91.56	13.61
(pH=7.3)	0.5	0.42	84.99	16.19

388 *RSD represents relative standard deviation calculated from duplicates.*

### 389 **3.5. Biosensor Specificity and Stability**

390 To ascertain the specificity of the developed electrochemical biosensor, homologous genes  
 391 from MPXV and vaccinia virus (VACV) were employed as the target and control,  
 392 respectively. The biosensor showed a specific electrochemical response for MPXV target  
 393 with no evident cross-reactivity (**Fig. 4A**). These findings suggest that our electrochemical  
 394 system can reliably detect MPXV.

395 The storage stability of the biosensor was investigated under different storage conditions  
396 at room temperature. The ssDNA-modified SPEs were stored in a nitrogen gas-protected

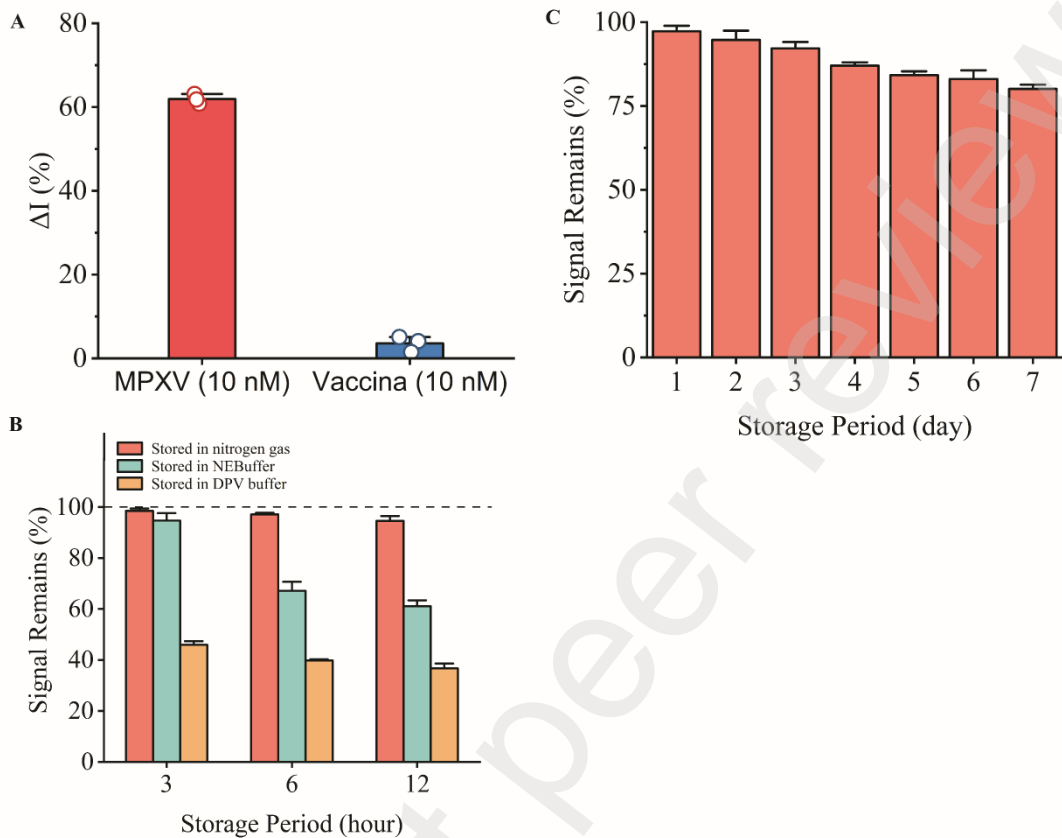


Fig. 4 Specificity and stability of the developed biosensor. (A) Specificity analysis of the developed biosensor; (B and C) Storage stability of the ssDNA-modified electrodes. Error bars indicate standard deviation calculated from three independent measurements ( $n=3$ ).

397 environment, in NEbuffer, and DPV buffer at room temperature. Three electrodes were  
398 used for each tested condition. It was observed that under nitrogen gas-protected  
399 environment (vacuum created by nitrogen gas), ssDNA-modified electrodes retained 95%  
400 of the original signal within 12 hours (Fig. 4B) while the electrodes stored in NEbuffer and  
401 DPV buffer rapidly lost their signal retention. We thus used nitrogen gas-protected  
402 environment to test the storage stability for an extended period. The biosensor showed a  
403 slight deviation in signal for the first 3 days which was subsequently reduced to ~80% of  
404 the original signal after 7 days of storage at room temperature (Fig. 4C), indicating  
405 promising storage stability. Regardless of being an important parameter for practical utility  
406 of biosensors, very few studies report on the storage stability of electrochemical biosensors.  
407 Our sensor demonstrated an excellent storage stability compared to a related biosensor [32].

408 **3.6. Method Comparison**

409 To evaluate the consistency between our proposed CRISPR-based electrochemical  
410 biosensor and widely accepted fluorescence-based detection method, DNA extracted from  
411 the environmental water samples spiked with MPXV pseudovirus was used as a positive

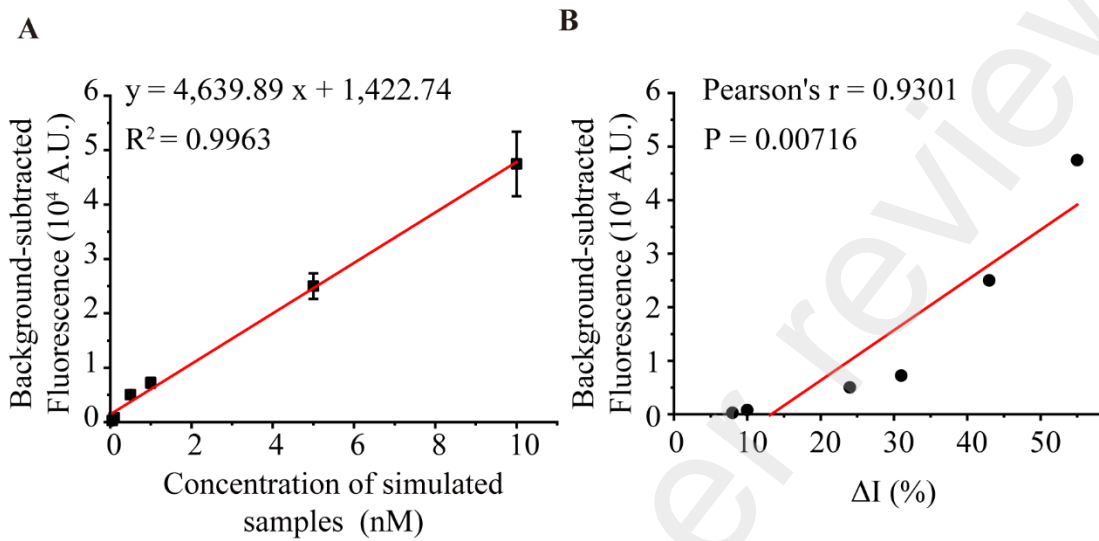


Figure 5 Method comparison for the evaluation of reliability of the proposed system. (A) Calibration curve obtained using microplate reader method; (B) Consistency between electrochemical biosensor and microplate reader results for MPXV detection.

412 sample. A series of concentrations was tested using microtiter plate reader, and a  
413 calibration curve was obtained (Fig. 5A). A similar curve was also obtained using our  
414 biosensor. Using plate reader and our proposed biosensor data, the Pearson correlation  
415 coefficient was computed to evaluate the correlation between two methods (Fig. 5B). The  
416 Pearson's  $r = 0.9301$  and  $p = 0.00716$  were obtained. These results indicate that our  
417 proposed method is consistent with the fluorescence-based detection technique, further  
418 demonstrating the reliability of our electrochemical biosensor for MPXV detection in  
419 wastewater.

420 **4. Conclusions**

421 Herein, we successfully developed and demonstrated a prototype biosensing system for  
422 mpox detection in wastewater samples. The proposed approach is destined to inform health  
423 authorities about disease propagation scale at community level without impacting the  
424 normal activities of general population as no mass clinical testing is required for data  
425 collection. This study experimentally shows that the CRISPR/Cas system can  
426 electrochemically detect MPXV DNA in human saliva, tap water, river water, and sea

427 water with a satisfactory accuracy. The spike-recovery tests showing 85-103% recoveries  
428 indicate the feasibility and applicability of our system for wastewater surveillance  
429 programs. Moreover, the integration of IoT platform with biosensing system makes our  
430 approach amenable to integration with ongoing wastewater surveillance programs for  
431 infectious diseases. Owing to the programmable nature of crRNA and availability of a  
432 multitude of CRISPR systems, our electrochemical biosensor can also serve as a versatile  
433 sensing tool for detection of other pathogens with slight modifications to the existing set  
434 up.

435

#### 436 **Author Contribution**

437 “**Xiaoyun Zhong:** Conceptualization, Methodology, Formal Analysis, Data Curation, Writing Original Draft.  
438 **Ijaz Gul:** Original Idea, Conceptualization, Methodology, Validation, Supervision, Writing-Original Draft,  
439 Writing-Review & Editing. **Xi Yuan:** Validation. **Muhammad Akmal Raheem:** Writing-Review &  
440 Editing. **Ke Lin:** Writing-Review & Editing. **Chenying Lu:** Writing-Review & Editing. **Junguo Hui:**  
441 Writing-Review & Editing. **Shuiwei Xia:** Writing-Review & Editing. **Minjiang Chen:** Writing-Review &  
442 Editing. **Min Xu:** Writing-Review & Editing. **Lin Shen:** Writing-Review & Editing. **Zhenglin Chen:**  
443 Writing-Review & Editing. **Chenggang Yan:** Writing-Review & Editing. **Peiwu Qin:** Supervision,  
444 Resources, Funding Acquisition, Project Administration, Writing-Review & Editing. **Dongmei Yu:**  
445 Supervision. **Jiansong Ji:** Supervision”.

#### 446 **Acknowledgement**

447 “We gratefully acknowledge funding from the National Natural Science Foundation of China  
448 31970752,32350410397; Science, Technology, Innovation Commission of Shenzhen Municipality,  
449 JCYJ20220530143014032, JCYJ20230807113017035, WDZC20200820173710001, Shenzhen Medical  
450 Research Funds, D2301002; Department of Chemical Engineering-iBHE Special Cooperation Joint Fund  
451 Project, DCE-iBHE-2022-3; Tsinghua Shenzhen International Graduate School Cross-disciplinary Research  
452 and Innovation Fund Research Plan, JC2022009; and Bureau of Planning, Land and Resources of Shenzhen  
453 Municipality, (2022) 207.”

#### 454 **Declaration of Competing Interest**

455 All authors declare that they have no conflict of interest.

#### 456 **Ethical Approval**

457 This study does not involve any human or animal samples.

458    **References**

- 459    [1] WHO, Monkeypox declared a global health emergency by the World Health  
460    Organization, (2022).  
461    <https://news.un.org/en/story/2022/07/1123152#:~:text=Monkeypox%20declared%20a>  
462    global health emergency by the,... 2 Undecided committee. ... 3 Recommendations.  
463    (accessed May 9, 2024).
- 464    [2] I. Gul, C. Liu, X. Yuan, Z. Du, S. Zhai, Z. Lei, Q. Chen, M.A. Raheem, Q. He, Q.  
465    Hu, C. Xiao, Z. Haihui, R. Wang, S. Han, K. Du, D. Yu, C.Y. Zhang, P. Qin,  
466    Current and Perspective Sensing Methods for Monkeypox Virus, *Bioengineering*.  
467    9 (2022). <https://doi.org/10.3390/bioengineering9100571>.
- 468    [3] WHO, WHO Director-General's opening remarks at the media briefing – 11 May  
469    2023, (2023). <https://www.who.int/director-general/speeches/detail/who-director-general-s-opening-remarks-at-the-media-briefing---11-may-2023> (accessed May 9,  
471    2024).
- 472    [4] J. Lu, H. Xing, C. Wang, M. Tang, C. Wu, F. Ye, L. Yin, Y. Yang, W. Tan, L.  
473    Shen, Mpox (formerly monkeypox): pathogenesis, prevention, and treatment,  
474    *Signal Transduct. Target. Ther.* 8 (2023) 458. <https://doi.org/10.1038/s41392-023-01675-2>.
- 476    [5] H. Guan, I. Gul, C. Xiao, S. Ma, Y. Liang, D. Yu, Y. Liu, H. Liu, C.Y. Zhang, J.  
477    Li, P. Qin, Emergence, phylogeography, and adaptive evolution of mpox virus,  
478    *New Microbes New Infect.* 52 (2023) 101102.  
479    [https://doi.org/https://doi.org/10.1016/j\\_nmni.2023.101102](https://doi.org/https://doi.org/10.1016/j_nmni.2023.101102).
- 480    [6] E.F. Alakunle, M.I. Okeke, Monkeypox virus: a neglected zoonotic pathogen  
481    spreads globally, *Nat. Rev. Microbiol.* 20 (2022) 507–508.  
482    <https://doi.org/10.1038/s41579-022-00776-z>.
- 483    [7] D. Pan, J. Nazareth, S. Sze, C.A. Martin, J. Decker, E. Fletcher, T. Déirdre  
484    Hollingsworth, M.R. Barer, M. Pareek, J.W. Tang, Transmission of  
485    monkeypox/mpox virus: A narrative review of environmental, viral, host, and  
486    population factors in relation to the 2022 international outbreak, *J. Med. Virol.* 95  
487    (2023) e28534. <https://doi.org/https://doi.org/10.1002/jmv.28534>.
- 488    [8] A. Peiró-Mestres, I. Fuertes, D. Camprubí-Ferrer, M.Á. Marcos, A. Vilella, M.  
489    Navarro, L. Rodriguez-Elena, J. Riera, A. Català, M.J. Martínez, J.L. Blanco, on  
490    behalf of the Hospital Clinic de Barcelona Monkeypox Study Group, Frequent  
491    detection of monkeypox virus DNA in saliva, semen, and other clinical samples  
492    from 12 patients, Barcelona, Spain, May to June 2022, *Eurosurveillance*. 27  
493    (2022). <https://doi.org/https://doi.org/10.2807/1560-7917.ES.2022.27.28.2200503>.
- 494    [9] A. Antinori, V. Mazzotta, S. Vita, F. Carletti, D. Tacconi, L.E. Lapini, A.  
495    D'Abramo, S. Cicalini, D. Lapa, S. Pittalis, V. Puro, M. Rivano Capparuccia, E.  
496    Giombini, C.E.M. Gruber, A.R. Garbuglia, A. Marani, F. Vairo, E. Girardi, F.  
497    Vaia, E. Nicastri, the INMI Monkeypox Group, Epidemiological, clinical and  
498    virological characteristics of four cases of monkeypox support transmission

- 499 through sexual contact, Italy, May 2022, *Eurosurveillance*. 27 (2022).  
500 <https://doi.org/https://doi.org/10.2807/1560-7917.ES.2022.27.22.2200421>.
- 501 [10] A. Atoui, F. Jourdain, D. Mouly, C. Cordevant, T. Chesnot, B. Gassilloud, A  
502 review on mpox (monkeypox) virus shedding in wastewater and its persistence  
503 evaluation in environmental samples, *Case Stud. Chem. Environ. Eng.* 7 (2023)  
504 100315. <https://doi.org/https://doi.org/10.1016/j.cscee.2023.100315>.
- 505 [11] R. Maal-Bared, C. Gerba, K. Bibby, N. Munakata, A.S. Mehrotra, K.F. Brisolara,  
506 C. Haas, L. Gary, B. Nayak, J. Swift, S. Sherchan, L. Casson, L. Olabode, A.  
507 Rubin, R. Reimers, M. Sobsey, The Current Multicountry Monkeypox Outbreak:  
508 What Water Professionals Should Know, *ACS ES\&T Water*. 2 (2022) 1628–  
509 1638. <https://doi.org/10.1021/acsestwater.2c00287>.
- 510 [12] S. Wurtzer, M. Levert, E. Dhenain, M. Boni, J.N. Tournier, N. Londinsky, A.  
511 Lefranc, O. and Ferraris, L. Moulin, First Detection of Monkeypox Virus Genome  
512 in Sewersheds in France: The Potential of Wastewater-Based Epidemiology for  
513 Monitoring Emerging Disease, *Environ. Sci. \& Technol. Lett.* 9 (2022) 991–996.  
514 <https://doi.org/10.1021/acs.estlett.2c00693>.
- 515 [13] E.F. de Jonge, C.M. Peterse, J.M. Koelewijn, A.-M.R. van der Drift, R.F.H.J. van  
516 der Beek, E. Nagelkerke, W.J. Lodder, The detection of monkeypox virus DNA in  
517 wastewater samples in the Netherlands, *Sci. Total Environ.* 852 (2022) 158265.  
518 <https://doi.org/https://doi.org/10.1016/j.scitotenv.2022.158265>.
- 519 [14] G. La Rosa, P. Mancini, C. Veneri, G.B. Ferraro, L. Lucentini, M. Iaconelli, E.  
520 Suffredini, Detection of Monkeypox Virus DNA in Airport Wastewater, Rome,  
521 Italy, *Emerg. Infect. Dis.* 29 (2023) 193–196.  
522 <https://doi.org/10.3201/eid2901.221311>.
- 523 [15] A. Tiwari, S. Adhikari, D. Kaya, M.A. Islam, B. Malla, S.P. Sherchan, A.I. Al-  
524 Mustapha, M. Kumar, S. Aggarwal, P. Bhattacharya, K. Bibby, R.U. Halden, A.  
525 Bivins, E. Haramoto, S. Oikarinen, A. Heikinheimo, T. Pitkänen, Monkeypox  
526 outbreak: Wastewater and environmental surveillance perspective, *Sci. Total  
527 Environ.* 856 (2023) 159166.  
528 <https://doi.org/https://doi.org/10.1016/j.scitotenv.2022.159166>.
- 529 [16] C. Bagutti, M. Alt Hug, P. Heim, E. Ilg Hampe, P. Hübner, T.R. Julian, K.N.  
530 Koch, K. Grosheintz, M. Kraus, C. Schaubhut, R. Tarnutzer, E. Würfel, S. Fuchs,  
531 S. Tschudin-Sutter, Association between the number of symptomatic mpox cases  
532 and the detection of mpox virus DNA in wastewater in Switzerland: an  
533 observational surveillance study, *Swiss Med. Wkly.* 154 (2024) 3706.  
534 <https://doi.org/10.57187/s.3706>.
- 535 [17] J. Xu, C. Liu, Q. Zhang, H. Zhu, F. Cui, Z. Zhao, M. Song, B. Zhou, Y. Zhang, P.  
536 Hu, L. Li, Q. Wang, P. Wang, The first detection of mpox virus DNA from  
537 wastewater in China, *Sci. Total Environ.* 932 (2024) 172742.  
538 <https://doi.org/https://doi.org/10.1016/j.scitotenv.2024.172742>.
- 539 [18] Q. Chen, I. Gul, C. Liu, Z. Lei, X. Li, M.A. Raheem, Q. He, Z. Haihui, E.

- 540 Leeansyah, C.Y. Zhang, V. Pandey, K. Du, P. Qin, CRISPR–Cas12-based field-  
541 deployable system for rapid detection of synthetic DNA sequence of the  
542 monkeypox virus genome, *J. Med. Virol.* 95 (2023) e28385.  
543 <https://doi.org/https://doi.org/10.1002/jmv.28385>.
- 544 [19] Y. Sui, Q. Xu, M. Liu, K. Zuo, X. Liu, J. Liu, CRISPR-Cas12a-based detection of  
545 monkeypox virus, *J. Infect.* (2022). [https://doi.org/https://doi.org/10.1016/j.jinf.2022.08.043](https://doi.org/10.1016/j.jinf.2022.08.043).
- 546 [20] J.S. Stefano, L.R.G. e Silva, C. Kalinke, P.R. de Oliveira, R.D. Crapnell, L.C.  
547 Brazaca, J.A. Bonacin, S. Campuzano, C.E. Banks, B.C. Janegitz, Human  
548 monkeypox virus: Detection methods and perspectives for diagnostics, *TrAC*  
549 *Trends Anal. Chem.* 167 (2023) 117226.  
550 <https://doi.org/https://doi.org/10.1016/j.trac.2023.117226>.
- 551 [21] X. Song, Y. Tao, S. Bian, M. Sawan, Optical biosensing of monkeypox virus using  
552 novel recombinant silica-binding proteins for site-directed antibody  
553 immobilization, *J. Pharm. Anal.* (2024) 100995.  
554 <https://doi.org/10.1016/j.jpha.2024.100995>.
- 555 [22] J. Wu, H. Liu, W. Chen, B. Ma, H. Ju, Device integration of electrochemical  
556 biosensors, *Nat. Rev. Bioeng.* 1 (2023) 346–360. <https://doi.org/10.1038/s44222-023-00032-w>.
- 558 [23] M. Bahri, M. Amin Elaguech, S. Nasraoui, K. Djebbi, O. Kanoun, P. Qin, C. Tlili,  
559 D. Wang, Laser-Induced graphene electrodes for highly sensitive detection of  
560 DNA hybridization via consecutive cytosines (polyC)-DNA-based electrochemical  
561 biosensors, *Microchem. J.* 185 (2023) 108208.  
562 <https://doi.org/https://doi.org/10.1016/j.microc.2022.108208>.
- 563 [24] I. Gul, W. Le, Z. Jie, F. Ruiqin, M. Bilal, L. Tang, Recent advances on engineered  
564 enzyme-conjugated biosensing modalities and devices for halogenated compounds,  
565 *TrAC Trends Anal. Chem.* 134 (2021) 116145.  
566 <https://doi.org/10.1016/j.trac.2020.116145>.
- 567 [25] S. Singh, R. Thakran, A. Kaushal, R. V Saini, A. Saini, S. Datta, Crispr-Cas based  
568 biosensing: A fast-expanding molecular diagnostic tool, *Microchem. J.* 200 (2024)  
569 110421. <https://doi.org/https://doi.org/10.1016/j.microc.2024.110421>.
- 570 [26] M.M. Kaminski, O.O. Abudayyeh, J.S. Gootenberg, F. Zhang, J.J. Collins,  
571 CRISPR-based diagnostics, *Nat. Biomed. Eng.* 5 (2021) 643–656.  
572 <https://doi.org/10.1038/s41551-021-00760-7>.
- 573 [27] L. Wang, C. Xu, S. Zhang, S. Chen, H. Wang, Z. Duan, O.A. Al-Hartomy, S.  
574 Wageh, X. Wen, Y. Liu, Y. Lin, H. Pu, Z. Xie, Q. Liu, H. Zhang, D. Luo, Rapid  
575 and ultrasensitive detection of mpox virus using CRISPR/Cas12b-empowered  
576 graphene field-effect transistors, *Appl. Phys. Rev.* 10 (2023).  
577 <https://doi.org/10.1063/5.0142494>.
- 578 [28] F. Zhao, Y. Hu, Z. Fan, B. Huang, L. Wei, Y. Xie, Y. Huang, S. Mei, L. Wang, L.  
579 Wang, B. Ai, J. Fang, C. Liang, F. Xu, W. Tan, F. Guo, Rapid and sensitive one-  
580 tube detection of mpox virus using RPA-coupled CRISPR-Cas12 assay, *Cell*

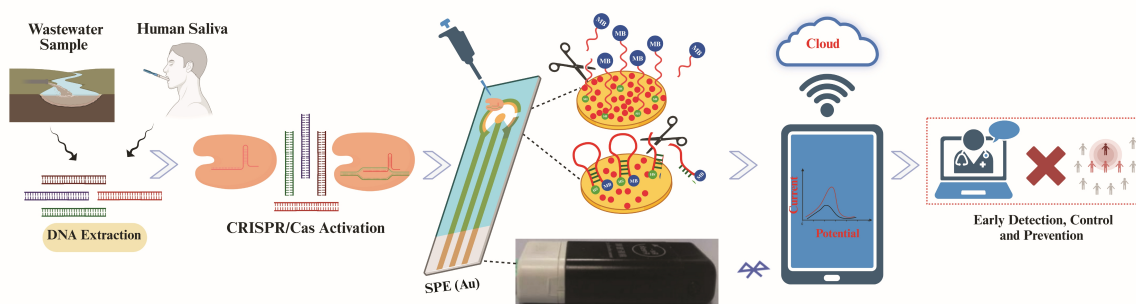
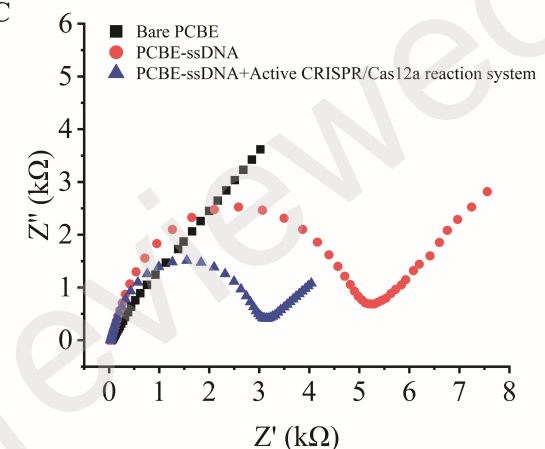
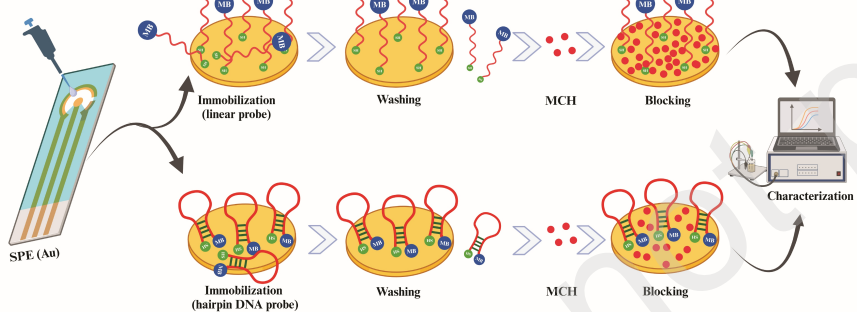
- 581 Reports Methods. 3 (2023) 100620. <https://doi.org/10.1016/j.crmeth.2023.100620>.
- 582 [29] C. Han, Q. Liu, X. Luo, J. Zhao, Z. Zhang, J. He, F. Ge, W. Ding, Z. Luo, C. Jia,  
583 L. Zhang, Development of a CRISPR/Cas12a-mediated aptasensor for Mpox virus  
584 antigen detection, Biosens. Bioelectron. 257 (2024) 116313.  
585 <https://doi.org/10.1016/j.bios.2024.116313>.
- 586 [30] X. Wang, X. Deng, Y. Zhang, W. Dong, Q. Rao, Q. Huang, F. Tang, R. Shen, H.  
587 Xu, Z. Jin, Y. Tang, D. Du, A rapid and sensitive one-pot platform integrating  
588 fluorogenic RNA aptamers and CRISPR-Cas13a for visual detection of  
589 monkeypox virus, Biosens. Bioelectron. 257 (2024) 116268.  
590 <https://doi.org/10.1016/j.bios.2024.116268>.
- 591 [31] Y. Yang, F. Gong, X. Shan, Z. Tan, F. Zhou, X. Ji, M. Xiang, F. Wang, Z. He,  
592 Amplification-free detection of Mpox virus DNA using Cas12a and multiple  
593 crRNAs, Microchim. Acta. 191 (2024) 102. <https://doi.org/10.1007/s00604-024-06184-9>.
- 595 [32] L.F. de Lima, P.P. Barbosa, C.L. Simeoni, R.F. de O. de Paula, J.L. Proenca-  
596 Modena, W.R. de Araujo, Electrochemical Paper-Based Nanobiosensor for Rapid  
597 and Sensitive Detection of Monkeypox Virus, ACS Appl. Mater. Interfaces. 15  
598 (2023) 58079–58091. <https://doi.org/10.1021/acsami.3c10730>.
- 599 [33] M. Chandran, G. Chellasamy, M. Veerapandian, B. Dhanasekaran, S. Kumar  
600 Arumugasamy, S. Govindaraju, K. Yun, Fabrication of label-free immunoprobe  
601 for monkeypox A29 detection using one-step electrodeposited molybdenum oxide-  
602 graphene quantum rods, J. Colloid Interface Sci. 660 (2024) 412–422.  
603 <https://doi.org/https://doi.org/10.1016/j.jcis.2023.12.188>.
- 604 [34] S. Cai, R. Ren, J. He, X. Wang, Z. Zhang, Z. Luo, W. Tan, Y. Korchev, J.B. Edel,  
605 A.P. Ivanov, Selective Single-Molecule Nanopore Detection of mpox A29 Protein  
606 Directly in Biofluids, Nano Lett. 23 (2023) 11438–11446.  
607 <https://doi.org/10.1021/acs.nanolett.3c02709>.
- 608 [35] Z. Chen, F. Li, L. Zhang, Z. Lei, C. Yang, C. Xiao, L. Lian, X. Yuan, G. Ijaz, J.  
609 Yang, Z. Lin, Y. He, P. Zhang, D. Yu, P. Qin, Temperature tolerant all-solid-state  
610 touch panel with high stretchability, transparency and self-healing ability, Chem.  
611 Eng. J. 451 (2023) 138672.  
612 <https://doi.org/https://doi.org/10.1016/j.cej.2022.138672>.
- 613 [36] M. Bahri, Z. Fredj, P. Qin, M. Sawan, DNA-Coupled AuNPs@CuMOF for  
614 Sensitive Electrochemical Detection of Carcinoembryonic Antigen, ACS Appl.  
615 Nano Mater. 7 (2024) 11921–11930. <https://doi.org/10.1021/acsanm.4c01473>.
- 616 [37] J. Xu, J. Ma, Y. Li, L. Kang, B. Yuan, S. Li, J. Chao, L. Wang, J. Wang, S. Su, Y.  
617 Yuan, A general RPA-CRISPR/Cas12a sensing platform for Brucella spp.  
618 detection in blood and milk samples, Sensors Actuators B Chem. 364 (2022)  
619 131864. <https://doi.org/https://doi.org/10.1016/j.snb.2022.131864>.
- 620 [38] D. Zhang, Y. Yan, H. Que, T. Yang, X. Cheng, S. Ding, X. Zhang, W. Cheng,  
621 CRISPR/Cas12a-Mediated Interfacial Cleaving of Hairpin DNA Reporter for



- 663 collected during the 2022 mpox outbreak in Lombardy, Italy, *Travel Med. Infect.*  
664 *Dis.* 59 (2024) 102698.  
665 <https://doi.org/https://doi.org/10.1016/j.tmaid.2024.102698>.
- 666 [48] R. Palich, S. Burrel, G. Monsel, A. Nouchi, A. Bleibtreu, S. Seang, V. Bérot, C.  
667 Brin, A. Gavaud, Y. Wakim, N. Godefroy, A. Fayçal, Y. Tamzali, T. Grunemwald,  
668 M. Ohayon, E. Todesco, V. Leducq, S. Marot, V. Calvez, A.-G. Marcelin, V.  
669 Pourcher, Viral loads in clinical samples of men with monkeypox virus infection: a  
670 French case series, *Lancet Infect. Dis.* 23 (2023) 74–80.  
671 [https://doi.org/https://doi.org/10.1016/S1473-3099\(22\)00586-2](https://doi.org/https://doi.org/10.1016/S1473-3099(22)00586-2).
- 672 [49] G. Can, B. Perk, B.E. Çitil, Y.T. Büyüksünetçi, Ü. Anık, Electrochemical  
673 Immunoassay Platform for Human Monkeypox Virus Detection, *Anal. Chem.* 0  
674 (n.d.) null. <https://doi.org/10.1021/acs.analchem.3c05182>.
- 675 [50] A. Saha, M. Ahsan, P.R. Arantes, M. Schmitz, C. Chanze, M. Jinek, G. Palermo,  
676 An alpha-helical lid guides the target DNA toward catalysis in CRISPR-Cas12a,  
677 *Nat. Commun.* 15 (2024) 1473. <https://doi.org/10.1038/s41467-024-45762-6>.
- 678 [51] X. Tong, K. Zhang, Y. Han, T. Li, M. Duan, R. Ji, X. Wang, X. Zhou, Y. Zhang,  
679 H. Yin, Fast and sensitive CRISPR detection by minimized interference of target  
680 amplification, *Nat. Chem. Biol.* (2024). <https://doi.org/10.1038/s41589-023-01534-9>.
- 682 [52] A.V.S. Sarma, A. Anbanandam, A. Kelm, R. Mehra-Chaudhary, Y. Wei, P. Qin,  
683 Y. Lee, M. V Berjanskii, J.A. Mick, L.J. Beamer, S.R. Van Doren, Solution NMR  
684 of a 463-Residue Phosphohexomutase: Domain 4 Mobility, Substates, and  
685 Phosphoryl Transfer Defect, *Biochemistry*. 51 (2012) 807–819.  
686 <https://doi.org/10.1021/bi201609n>.
- 687 [53] I. Gul, T.F. Bogale, Y. Chen, X. Yang, R. Fang, J. Feng, H. Gao, L. Tang, A  
688 paper-based whole-cell screening assay for directed evolution-driven enzyme  
689 engineering, *Appl. Microbiol. Biotechnol.* 104 (2020) 6013–6022.  
690 <https://doi.org/10.1007/s00253-020-10615-x>.
- 691 [54] M. Bahri, D. Yu, C.Y. Zhang, Z. Chen, C. Yang, L. Douadji, P. Qin, Unleashing  
692 the potential of tungsten disulfide: Current trends in biosensing and nanomedicine  
693 applications, *Heliyon*. 10 (2024) e24427.  
694 <https://doi.org/10.1016/j.heliyon.2024.e24427>.
- 695 [55] N. Rohaizad, C.C. Mayorga-Martinez, M. Fojtů, N.M. Latiff, M. Pumera, Two-  
696 dimensional materials in biomedical{,} biosensing and sensing applications,  
697 *Chem. Soc. Rev.* 50 (2021) 619–657. <https://doi.org/10.1039/D0CS00150C>.
- 698 [56] D. Fan, X. Yuan, W. Wu, R. Zhu, X. Yang, Y. Liao, Y. Ma, C. Xiao, C. Chen, C.  
699 Liu, H. Wang, P. Qin, Self-shrinking soft demoulding for complex high-aspect-  
700 ratio microchannels, *Nat. Commun.* 13 (2022) 5083.  
701 <https://doi.org/10.1038/s41467-022-32859-z>.
- 702 [57] C. Wang, P. Qin, D. Lv, J. Wan, S. Sun, H. Ma, Characterization of anisotropy of  
703 the porous anodic alumina by the Mueller matrix imaging method, *Opt. Express*.

- 704 28 (2020) 6740–6754. <https://doi.org/10.1364/OE.380070>.
- 705 [58] J. Moon, C. Liu, Asymmetric CRISPR enabling cascade signal amplification for  
706 nucleic acid detection by competitive crRNA, *Nat. Commun.* 14 (2023) 7504.  
707 <https://doi.org/10.1038/s41467-023-43389-7>.
- 708 [59] H. Chen, E. Kätelhön, R.G. Compton, Machine learning in fundamental  
709 electrochemistry: Recent advances and future opportunities, *Curr. Opin.*  
710 *Electrochem.* 38 (2023) 101214.  
711 <https://doi.org/https://doi.org/10.1016/j.coelec.2023.101214>.
- 712 [60] R. Zhang, X. Han, Z. Lei, C. Jiang, I. Gul, Q. Hu, S. Zhai, H. Liu, L. Lian, Y. Liu,  
713 Y. Zhang, Y. Dong, C.Y. Zhang, T.K. Lam, Y. Han, D. Yu, J. Zhou, P. Qin,  
714 RCMNet: A deep learning model assists CAR-T therapy for leukemia, *Comput.*  
715 *Biol. Med.* 150 (2022) 106084.  
716 <https://doi.org/10.1016/j.compbioemed.2022.106084>.

717

**A****C****B****D**